International Journal of Nanomedicine

Dovepress
open access to scientific and medical research

Open Access Full Text Article

ORIGINAL RESEARCH

Celastrol nanomicelles attenuate cytokine secretion in macrophages and inhibit macrophage-induced corneal neovascularization in rats

This article was published in the following Dove Press journal:
International Journal of Nanomedicine
18 November 2016
Number of times this article has been viewed

Zhanrong Li[1,*]
Jingguo Li[1,*]
Lei Zhu[1]
Ying Zhang[1]
Junjie Zhang[1]
Lin Yao[2]
Dan Liang[2]
Liya Wang[1]

[1]Henan Eye Institute, Henan Eye Hospital, Henan Provincial People's Hospital and Zhengzhou University People's Hospital, Zhengzhou, [2]State Key Laboratory of Ophthalmology, Zhongshan Ophthalmic Center, Sun Yat-Sen University, Guangzhou, People's Republic of China

*These authors contributed equally to this work

Abstract: The aim of the present study was to investigate the inhibitory effects of celastrol-loaded nanomicelles (CNMs) on activated macrophage-induced corneal neovascularization (CNV) in rats and cytokine secretion in macrophages. Using an angiogenesis assay in vitro, we detected the effects of CNMs on human umbilical vein endothelial cell (HUVEC) migration and invasion. In addition, the expression levels of cytokines secreted from hypoxia-induced macrophages were assessed through cytokine array analysis. The expression of hypoxia-inducible factors-1α (HIF-1α), nuclear factor-kappa B p65 (NF-κB p65), phospho-nuclear factor-kappa B p65 (phospho-NF-κB p65), p38 mitogen-activated protein kinase (p38 MAPK), phospho-p38 MAPK, extracellular signal-regulated kinase 1/2 (ERK1/2), and phospho-ERK1/2 was analyzed by western blotting. Activated macrophages were elicited through mineral oil lumbar injection, labeled with 1,19-dioctadecyl-3-3-39,39-tetramethylindocarbocyanine (DiI) and implanted into the corneal micro-pocket to induce CNV and to assess the antiangiogenic effect in rats. CNV was morphometrically analyzed using ImageJ software. Histopathological features were evaluated by immunofluorescence immunostaining for vascular endothelial growth factor (VEGF) and matrix metalloproteinase-9 (MMP-9) on day 2 after surgery. In the present study, the results indicated that CNMs significantly inhibited the migration and invasion of HUVECs; remarkably attenuated the expression of VEGF, tumor necrosis factor-α, interleukin-1α, monocyte chemoattractant protein 1, cytokine-induced neutrophil chemoattractant 3, and MMP-9 protein; and downregulated ERK1/2, p38 MAPK, NF-κB activation, and HIF-1α expression in macrophages. The peritoneal cells elicited using mineral oil were highly purified macrophages, and the length and area of CNV were significantly decreased in the CNMs group compared with the control group. There was a significant reduction in the expression of VEGF and MMP-9 in activated macrophages and corneal tissue after pretreatment with CNMs in this model. In conclusion, CNMs potently suppressed macrophage-induced CNV via the inhibition of VEGF and MMP-9 expression. This effect might be mediated through attenuating macrophages via HIF-1α, MAPK, and NF-κB signaling pathways.

Keywords: celastrol, nanomicelles, macrophages, corneal neovascularization

Introduction

Corneal neovascularization (CNV) can lead to vision loss, and this condition can be caused by infection, chemical burns, or contact lens wear. CNV is typically associated with inflammation or hypoxic stress.[1] The mechanisms of CNV have been investigated, and several angiogenic and inflammatory molecules are involved in this process, such as vascular endothelial growth factor (VEGF), basic fibroblast growth factor, tumor necrosis factor-α (TNF-α), interleukin-6 (IL-6), and matrix metalloproteinases (MMPs).[2–4]

Correspondence: Liya Wang
Henan Eye Institute, Henan Eye Hospital, Henan Provincial People's Hospital and Zhengzhou University People's Hospital, Zhengzhou 450003, People's Republic of China
Tel +86 371 8733 0492
Fax +86 371 20 8733 4825
Email wangliya_55@126.com

Dan Liang
State Key Laboratory of Ophthalmology, Zhongshan Ophthalmic Center, Sun Yat-Sen University, 54 Xianlie South Road, Guangzhou 510060, People's Republic of China
Tel +86 371 8733 0492
Fax +86 371 20 8733 4825
Email liangd2@mail.sysu.edu.cn

submit your manuscript | www.dovepress.com
Dovepress
http://dx.doi.org/10.2147/IJN.S117425

Macrophages play a crucial role in the modulation of corneal angiogenesis through the secretion of various inflammatory and proangiogenic mediators. In a previous study, we demonstrated that activated macrophages could induce obvious CNV in a rat corneal pocket model.[5]

Celastrol, a pentacyclic triterpene extracted from the root bark of *Tripterygium wilfordii* Hook F, exhibits potent anti-inflammatory and antiangiogenic activities.[6,7] This drug has been widely used to treat chronic inflammation, autoimmune diseases, and many types of cancer.[8,9] Recently, celastrol has also been demonstrated as a powerful anti-obesity agent.[10] Despite its potential beneficial bioactivity, further therapeutic application of celastrol is affected by its poor water solubility. In a previous study, we developed celastrol-loaded poly(ethylene glycol)-block-poly(ε-caprolactone) (PEG-b-PCL) nanomicelles to improve the hydrophilicity of this drug, and after subconjunctival injection, the results showed that celastrol-loaded nanomicelles (CNMs) significantly inhibited CNV through the suppression of macrophage infiltration.[11] However, the mechanisms underlying celastrol-induced macrophage inhibition in CNV were not completely understood. Therefore, the purpose of the present study was to investigate the potential efficacy and mechanisms of CNMs against CNV induced by activated macrophages in a rat corneal pocket model.

Materials and methods

Preparation of CNMs

Celastrol (Figure 1A) was purchased from the Shanghai Institute of Materia Medica, Chinese Academy of Sciences (Shanghai, People's Republic of China). The preparation of CNMs was performed as previously described.[11] Briefly, PEG-b-PCL (2,000:1,000, Mw/Mn =1.18, JCS Biopolytech, Toronto, Canada; 10 mg) and celastrol (2 mg) were mixed in chloroform (2 mL) and subsequently added drop-wise to deionized water (20 mL) under ultrasonic agitation using a Type 60 Sonic Dismembrator (Fisher Scientific, Pittsburgh, PA, USA). The organic solvent was then removed through vacuum distillation using a rotary evaporator to enable micelle formation. The samples were further concentrated and washed three times using a Millipore Centrifugal Filter Device (MW cutoff: 10,000 Da; Millipore, Billerica, MA, USA) to remove free celastrol dissolved in the micelle solution, followed by filtration with a syringe filter (pore size: 0.22 μm) to eliminate large polymers or celastrol aggregates. A schematic illustration of celastrol-loaded micelle formation is shown in Figure 1. The blank micelles were prepared using the same preparation conditions and procedure.

Cell preparation

The human vascular endothelial cells EA.hy 926 (American Type Culture Collection [ATCC], Manassas, VA, USA) were cultured in Dulbecco's Modified Eagle's Medium (DMEM) supplemented with 10% (v/v) fetal calf serum (FCS), 100 U/mL penicillin, 100 μg/mL streptomycin, and 4.5 g/mL glucose at 37°C in 5% CO_2. NR8383 (a rat macrophage cell-line, ATCC) cells were cultured in Ham's F12K medium containing 10% FCS, 100 U/mL penicillin, and 100 μg/mL streptomycin under the same conditions at 37°C in 5% CO_2.

Mineral oil-elicited macrophages were collected from the peritoneal cavity of Sprague-Dawley (SD) rats according to a previously described method.[5,12] Briefly, cells were isolated from peritoneal lavage fluid samples collected on day 4 after intraperitoneal injection of 1 mL of mineral oil. The cells were dispensed and cultured overnight in DMEM with 10% heat-inactivated FCS and maintained at 37°C and 5% CO_2 in an incubator.

Cell migration and invasion assays

A scratching assay was performed to detect vascular endothelial cell migration as previously described.[13] Briefly, human umbilical vein endothelial cells (HUVECs) were plated onto gelatin-coated 6-well plates. When the cells reached 90% confluence, the individual wells were incubated with medium containing 0.5% FCS for 6 hours. The cells were scratched with a pipette tip and subsequently washed with phosphate-buffered saline (PBS). After treatment with CNMs

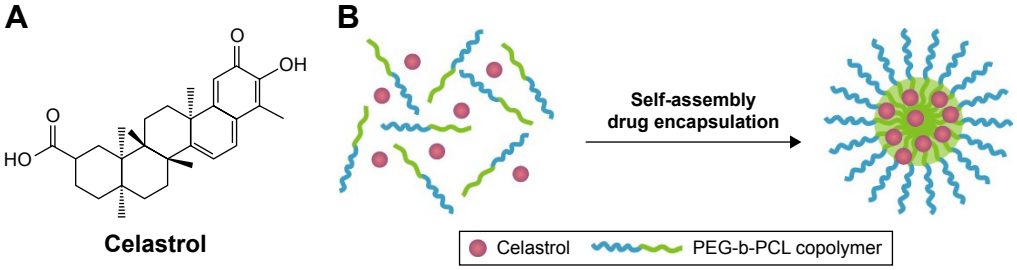

Figure 1 The chemical structures of (**A**) celastrol and (**B**) schematic illustration of celastrol nanomicelles formation.
Abbreviation: PEG-b-PCL, poly(ethylene glycol)-block-poly(ε-caprolactone).

(0, 13.6, and 27.2 μg/mL) for 10 hours, the cells that migrated toward the wound region were counted, and the percentage inhibition was expressed using untreated wells as 100%. The cell invasive assays were performed with 24-well 8-μm pore size Transwell chambers (Corning, Tewksbury, MA, USA). Briefly, 4×10^4 HUVECs were seeded into the upper chamber, which was coated with gelatin. The bottom wells were filled with 0.5% FCS medium containing different concentrations of CNMs (0, 13.6, and 27.2 μg/mL). After incubation for 8 hours, HUVECs in the top chamber were removed using a cotton swab. HUVECs that invaded to the bottom chamber were fixed with 4% paraformaldehyde and stained with 0.05% crystal violet. Crystal violet-positive invaded cells were counted. Percentage inhibition of invasive cells was expressed based on untreated control wells. Each experiment was performed in triplicate.

Rat cytokine antibody array

The amounts of secreted cytokines were compared between hypoxia-inducing macrophages with and without CNMs using the C-Series Rat Cytokine Antibody Array C1 for 19 rat cytokines (Ray Biotech, Norcross, GA, USA) as directed by the manufacturer. These macrophages (NR8383) are exposed to $CoCl_2$ to induce hypoxia. Briefly, after blocking with blocking buffer for 30 minutes, protein array membranes were incubated with ~2 mL of medium prepared from different macrophage samples with gentle shaking. After thoroughly washing, array membranes were incubated with diluted biotin-conjugated antibodies for 2 hours. Membranes were then washed and incubated with horseradish peroxidase (HRP)-conjugated streptavidin for 1 hour. Finally, signals were detected by the enhanced chemiluminescence system. The signal intensity of the spots was quantified using image software.

Western blot

NR8383 cells were treated with CNMs (0, 13.6, and 27.2 μg/mL) for 24 hours prior to determining MMP-9 protein expression. Hypoxic conditions were created by $CoCl_2$ (100 μM/mL). NR8383 cells were again exposed to CNMs (27.2 μg/mL) and further incubated for 24 hours prior to determining hypoxia-inducible factors-1α (HIF-1α), NF-κB p65, phospho-NF-κB p65, p38 MAPK, phospho-p38 MAPK, extracellular signal-regulated kinase 1/2 (ERK1/2), and phospho-ERK1/2 protein expression. The cells were harvested and lysed, and then the proteins were quantitatively analyzed using the bicinchoninic acid method (Thermo Scientific, Waltham, MA, USA). An equal amount of each protein sample was loaded onto sodium dodecyl sulfate gels and transferred to polyvinylidene difluoride membranes. After blocking with 5% nonfat dry milk at room temperature for 2 hours, the membranes were incubated with antibodies against MMP-9, HIF-1α, NF-κB p65, phospho-NF-κB p65, p38 MAPK, phospho-p38 MAPK, ERK1/2, phospho-ERK1/2, glyceraldehyde 3-phosphate dehydrogenase (GAPDH), and β-actin primary antibodies (Cell Signalling Technology, Danvers, MA, USA) overnight at 4°C. Subsequently, the membranes were washed and exposed to goat anti-rabbit-IgG HRP (Cell Signalling Technology) for 1 hour at room temperature, followed by imaging with a chemiluminescent substrate. The signal was analyzed using Image Lab (ECL). GAPDH and β-actin were used as loading controls.

The identification, purification, and trace of macrophages

The identification of macrophages from the peritoneal cavity was assayed through immunofluorescence staining. Briefly, cluster of differentiation 68 (CD68 or ED1, 1/100; Santa Cruz Biotechnology, Santa Cruz, CA, USA) was used as a primary antibody. Fluorescein isothiocyanate (FITC)-conjugated goat anti-mouse immunoglobulin G (Dako) was used as the secondary antibody. The nuclei were stained with 49, 6-diamidino-2-phenylindole-dihydrochloride (Sigma-Aldrich).

To analyze the purity and phagocytic activity of macrophages, FITC-dextran (Sigma-Aldrich) uptake studies were performed as previously described.[14] Briefly, macrophages were harvested, washed, and incubated with FITC-dextran (1 mg/mL) at 37°C for 1 hour. After incubation, the cells were washed twice with PBS, and the percentage of intracellular FITC-dextran was determined by flow cytometry (fluorescence-activated cell sorting [FACS]).

1,19-Dioctadecyl-3-3-39,39-tetramethylindocarbocyanine (DiI; Molecular Probes, Sigma-Aldrich) labeling was used to trace the implanted macrophages. The collected macrophages were labeled by incubation with 12.5 mg/mL DiI and then washed three times with PBS. Fluorescence signals were subsequently analyzed by FACS. In addition, the macrophages with immunofluorescence staining (CD68) were labeled with DiI and subsequently examined under confocal microscopy.

In vivo antiangiogenesis efficacy

All animal care and experimental protocols were approved by the Ethical Committee of Experimental Animal Care of Henan Eye Institute and complied with the National Institutes of Health guidelines, and all procedures in the study conformed to the Association for Research in Vision and Ophthalmology Statement for the Use of Animals in Ophthalmic

and Vision Research. To investigate whether CNMs inhibited CNV through the inhibition of macrophages, we used a rat corneal pocket model in which CNV was induced by activated macrophages. Adult female SD rats (200–220 g) were used. The right eye of each rat was selected for use in subsequent experiments. CNV was induced by activated macrophages in a corneal pocket model as previously described.[5] Briefly, the rats were anesthetized by intraperitoneal injection of 10% chloral hydrate (4 mL/kg). Then, the rat corneal pocket surgery was performed and ~1×10^4 homologous cells were implanted in each pocket. The animals were randomly divided into the activated macrophages (Mφ) group (n=5), CNMs treatment group (Mφ + CNMs), and the PBS group (Control). Harvested activated macrophages were pretreated with CNMs for 1 hour. CNV in each group was observed using the slit-lamp microscope each day prior to the death of animals from ketamine overdose on day 5. To evaluate the development of CNV, ink perfusion via the aorta was performed on day 5 as previously described.[15] The eyes were fixed overnight in 10% formalin, and then the fixed cornea was removed and flattened for image capture. Quantitative measurements of CNV length and area were assessed using Image Pro Plus 5.1 image analysis software (Media Cybernetics, Silver Spring, MD, USA).

In vivo imaging and corneal tissue immunochemistry

Fluorescence imaging provided an intuitive understanding with respect to the corneal pocket model. On day 1 after DiI-labeled macrophage implantation, the anesthetized animals were laid on a removable tray equipped with an imaging cabinet. The fluorescence images were recorded after applying the capture settings.

The expression of angiogenesis-related factors, such as VEGF and MMP-9, was detected in the cornea in every group by immunofluorescence staining. The eyes were enucleated for histological evaluation after rats were sacrificed on day 2. Frozen tissue sections were fixed in acetone. The primary antibodies were VEGF (Abcam) and MMP-9 (Abcam). FITC-conjugated goat anti-mouse immunoglobulin G was used as a secondary antibody. The cell nuclei were stained with 4′,6-diamidino-2-phenylindole-dihydrochloride. The stained corneal tissues were photographed using a confocal laser scanning microscope (Olympus BX60; Olympus, Tokyo, Japan).

Statistical analysis

The values were expressed as the mean ± standard deviation, and the difference between groups was analyzed using Student's *t*-test or one-way ANOVA with SPSS 16 software (SPSS Inc., Chicago, IL, USA). A *P*-value of <0.05 was considered statistically significant. The results are presented as (*) for probability <0.05 ($P<0.05$) and (**) for $P<0.01$.

Results and discussion

Formulation and characterization of CNMs

We developed the CNMs using ultrasonic agitation to improve the hydrophilicity and bioavailability of celastrol. The physicochemical properties of CNMs were examined in our previous study.[11,16] The results indicated that the micelles had an appropriate average hydrodynamic diameter of 48 nm, and a uniform spherical morphology was determined by SEM. The drug-loading content of CNMs was 7.36%, and the assessment of in vitro drug release revealed controlled release behavior.

To improve the bioavailability of celastrol, other carrier materials were developed, such as nanoencapsulation and lipid nanoparticles.[17,18] Furthermore, the developed CNMs could enhance the apparent aqueous solubility and improve the kinetic and thermodynamic stability in aqueous solution, compared with other carrier materials.[19] Moreover, the appropriate diameter (48 nm) and excellent amphipathic solubility of PEG-containing micelles might make it easy to penetrate the ocular barrier.[19] Therefore, polymeric nanomicelles might be better chosen as the celastrol delivery vector to further study the efficacy of CNMs in the treatment of ocular diseases.

CNMs suppressed cell migration, invasion, and angiogenesis in vitro

Previously, we demonstrated the effect of CNMs on inhibiting HUVEC proliferation and reducing endothelial tubule formation in vitro.[11] In the present study, we observed that treatment with CNMs resulted in the dose-dependent inhibition of HUVEC migration and invasion (Figure 2). Scratch test results showed that migration cell number was 101.63±2.81 in the blank micelles group (0 μg/mL) and 53.15±3.27 and 17.18±1.59 at different concentrations of CNMs (13.6 and 27.2 μg/mL, respectively, $*P<0.05$, $**P<0.01$; Figure 2A and B). The Transwell results showed that invasive cell number was 102.33±2.25 in the blank micelles group (0 μg/mL) and 48.67±2.63 and 11.50±1.15 at different concentrations of CNMs (13.6 and 27.2 μg/mL, respectively, $*P<0.05$, $**P<0.01$; Figure 2C and D). The migration and invasive cell numbers were not statistically significantly different between the control group and blank micelles group (0 μg/mL), whereas an obvious reduction

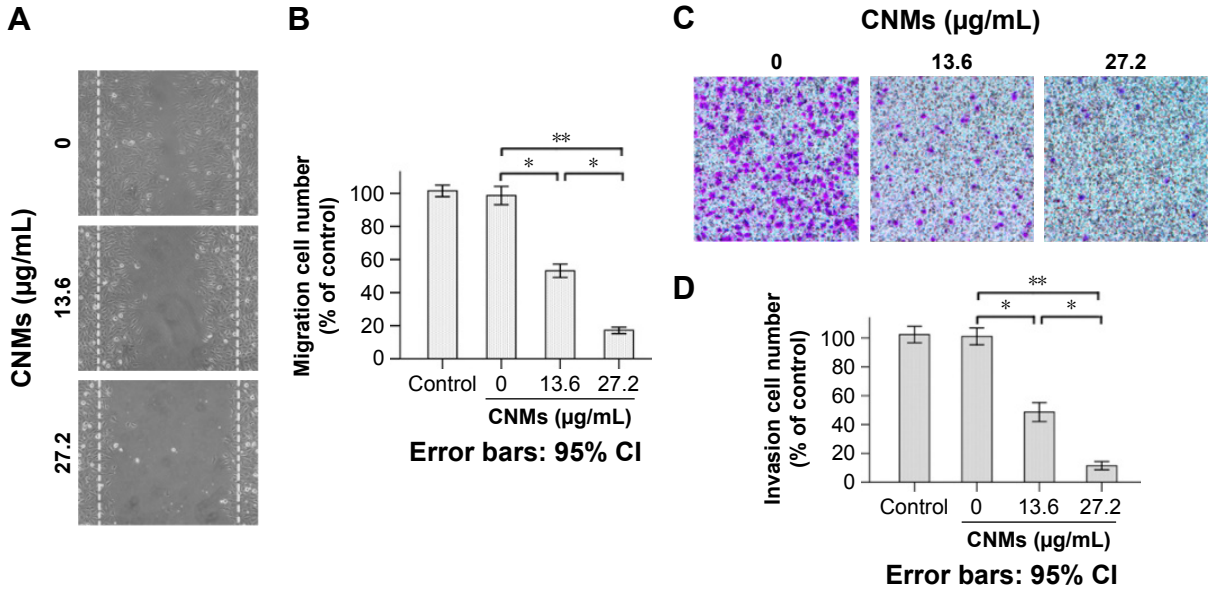

Figure 2 CNMs inhibit vascular endothelial cell migration and invasion in vitro.
Notes: (**A**) Cell migration. Representative images of CNMs inhibiting HUVEC migration in the scratching assay (×40). (**B**) The quantitative analysis of migration (*$P<0.05$, **$P<0.01$). (**C**) Cell invasion. Representative images of CNMs inhibiting HUVEC invasion in the Transwell chamber assay (×40). (**D**) The quantitative analysis of invasion (*$P<0.05$, **$P<0.01$).
Abbreviations: CI, confidence interval; CNMs, celastrol nanomicelles; HUVEC, human vascular endothelial cells.

was observed in the CNMs-treated (13.6 and 27.2 μg/mL) group compared with the control group and blank micelles group (0 μg/mL), indicating that the migration and invasion capacities of the cells after the treatment of CNMs treatment were significantly decreased.

Endothelial cell migration and invasion is an important step during angiogenesis. To assess the antiangiogenic property of CNMs in vitro, we examined its inhibitory effects on the chemotactic motility of endothelial cells using a well-established scratch migration assay and a Transwell assay. The results suggested that CNMs exhibit a statistically significant dose-related inhibition of HUVEC migration and invasion. In a previous study, we demonstrated the inhibitory effects of CNMs on HUVEC proliferation and capillary tubule formation in vitro. Together, these results indicated that CNMs could suppress angiogenesis in vitro through the inhibition of vascular endothelial cell proliferation, migration, invasion, and tubular structure formation, consistent with the results of previous similar studies.[20,21]

Effect of CNMs on the levels of cytokines in macrophages

The antibody array system was used to assess cytokine expression profiles mediated by CNMs in supernatants from hypoxia-induced macrophages harvested at 24 hours. As shown in Figure 3A–C, we simultaneously assessed the expression of 19 cytokines in CNM-treated hypoxia-induced macrophages. The results demonstrated that the expression of several of the 19 tested cytokines secreted from the hypoxia-induced macrophages, including cytokine-induced neutrophil chemoattractant 3 (CINC-3), monocyte chemoattractant protein 1 (MCP-1), VEGF, and TNF-α, was higher than that in untreated macrophages. Furthermore, their expression was suppressed following CNM treatment, particularly the expression of CINC-3, MCP-1, and VEGF, which was strongly decreased. In addition, the secretion of MCP-1, CINC-3, VEGF, and TNF-α was significantly increased under hypoxia, but was significantly decreased following CNM treatment compared with that in the untreated macrophages (Figure 3A and B, *$P<0.05$, **$P<0.01$). In contrast, the secretion of IL-1α was significantly increased under hypoxia, but was increased following CNM treatment compared with untreated macrophages (Figure 3A and B, *$P<0.05$, **$P<0.01$). However, little or no significant changes in the expression of the other cytokines were detected in the CNM-treated hypoxia-induced macrophages. Western blot analysis showed that the MMP-9 protein levels were significantly decreased by 0.41±0.02-fold and 0.13±0.02-fold in macrophages treated with 13.6 and 27.2 μg/mL CNMs, respectively (Figure 3D, *$P<0.05$, **$P<0.01$).

CNV is a condition that develops in response to inflammation and hypoxia stress.[1,22] Inflamed tissues are characterized by hypoxic conditions and immune cell infiltration. Macrophages have long been considered as important effector cells that

play a crucial role in corneal angiogenesis. In a previous study, we showed that activated macrophages could induce CNV.[5] Therefore, we assessed the inhibitory effect of CNMs on hypoxia-induced macrophages to identify the potential mechanism underlying their regulation of angiogenesis. The hypoxia mimetic $CoCl_2$ treatment can create hypoxia-like conditions and induce an inflammatory response.[23] Our present results demonstrated that $CoCl_2$ treatment increased the

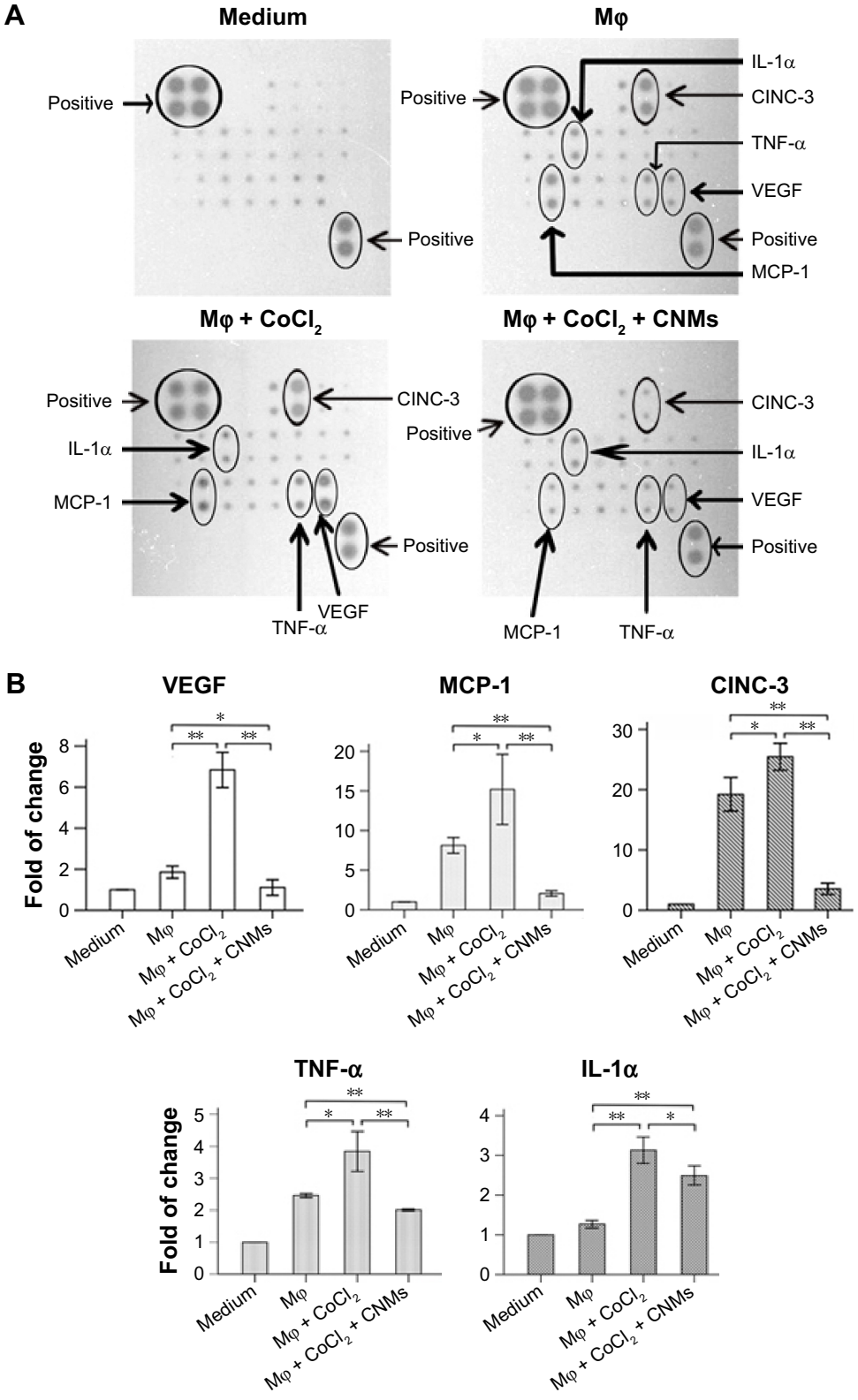

Figure 3 (*Continued*)

C

	A	B	C	D	E	F	G	H
1	POS	POS	NEG	NEG	CINC-2	CINC-3	CNTF	Fractalkine
2	POS	POS	NEG	NEG	CINC-2	CINC-3	CNTF	Fractalkine
3	GM-CSF	IFN gamma	IL-1 alpha	IL-1 beta	IL-4	IL-6	IL-10	LIX
4	GM-CSF	IFN gamma	IL-1 alpha	IL-1 beta	IL-4	IL-6	IL-10	LIX
5	Leptin	MCP-1	MIP-3 alpha	Beta NGF	TIMP-1	TNF alpha	VEGF	BLANK
6	Leptin	MCP-1	MIP-3 alpha	Beta NGF	TIMP-1	TNF alpha	VEGF	BLANK
7	BLANK	BLANK	BLANK	BLANK	BLANK	BLANK	BLANK	POS
8	BLANK	BLANK	BLANK	BLANK	BLANK	BLANK	BLANK	POS

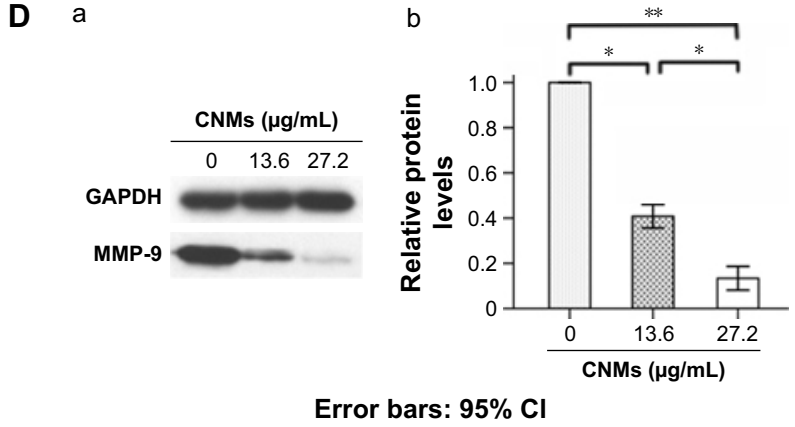

Figure 3 CNMs inhibit cytokine protein expression in Mφ.

Notes: (**A**) Detection of cytokine expression profiles in supernatants from hypoxia-inducing Mφ after CNMs treatment. Supernatants from Mφ treated with $CoCl_2$ (100 μM/mL) or $CoCl_2$ (100 μM/mL) + CNMs (27.2 μg/mL) for 24 hours and normal medium (control) were assessed using a rat cytokine antibody array. The downregulation of MCP-1, VEGF, TNF-α, and IL-1α was shown in the supernatants from hypoxia-inducing Mφ after CNMs treatment. (**B**) Statistical analysis of relative protein levels of cytokines. Mean optic densities of protein were calculated by normalizing to controls. The data indicate the mean ± SEM (n=3), *$P<0.05$ and **$P<0.01$. (**C**) Template showing the location of cytokine antibodies spotted onto the Rat Cytokine Array C1. (**D**) CNMs inhibit MMP-9 protein levels. Mφ (NR8383) were treated with CNMs for 24 hours at the indicated concentrations. Subsequently, (a) MMP-9 was detected by Western blotting, and (b) Statistical analysis of relative protein levels of MMP-9 *$P<0.05$ and **$P<0.01$.

Abbreviations: CI, confidence interval; CINC-3, cytokine-induced neutrophil chemoattractant 3; CNMs, celastrol nanomicelles; CNTF, ciliary neurotrophic factor; GM-CSF, granulocyte-macrophage colony-stimulating factor; IFN, interferon; IL-1α, interleukin-1α; Mφ, macrophages; MCP-1, monocyte chemotactic protein-1; MMP-9, matrix metalloproteinases 9; NEG, negative; POS, positive; TNF-α, tumor necrosis factor-α; VEGF, vascular endothelial growth factor; MIP-3 alpha, macrophage inflammatory protein 3 alpha.

expression of proangiogenesis cytokines, such as VEGF and TNF-α, and chemokines, such as MCP-1 and CINC-3, and this finding implied that these molecules might be involved in the development and maintenance of angiogenesis.

Macrophages can promote angiogenesis via several potential mechanisms in different phases of the angiogenic process.[24] First, the degradation of extracellular matrix via MMPs from macrophages enables vascular endothelium cell migration and the formation of new capillaries. MMP-9, as one of the main members of the MMPs family, is a potent proangiogenic factor involved in CNV progression. The inhibition of the activity and expression of MMP-9 significantly decreases CNV,[11,25] and subsequently, macrophages secrete various proangiogenic cytokines, such as VEGF and TNF-α, which directly or indirectly stimulate endothelial proliferation, migration, or tube formation.[2] VEGF is a major mediator of angiogenesis and is crucially involved in the development of CNV.[26] VEGF also increases vascular leakage and promotes monocyte chemotaxis in mice, indicating a key role for VEGF in inflammation.[3] As an endogenous proangiogenic factor, VEGF has been identified and isolated from cornea and tears.[27] Furthermore, VEGF inhibitors have exhibited potential for the treatment of CNV.[28] In addition, macrophages synthesize and release several chemokines, such as MCP-1, which attract more monocytes to form a macrophage amplification circuit.[29] CINC-3, a small molecule cytokine, can promote leukocyte invasion into the inflamed tissue.[30] In the present study, we demonstrated that CNMs could inhibit the expression of VEGF, MMP-9, TNF-α, MCP-1, and CINC-3 in macrophages. These results indicate the immune modulating effect of CNMs on macrophages and its antiangiogenic and anti-inflammatory activity.

CNMs inhibit the HIF-1α, NF-κB, and MAPK pathways in hypoxia-induced macrophages

Western blot analysis showed that HIF-1α, NF-κB p65, phospho-NF-κB p65, p38 MAPK, and phospho-p38 MAPK expression was increased in hypoxia-induced macrophages compared with normal macrophages. In addition, expression of HIF-1α, NF-κB, and the MAPK pathway was decreased in CNM-treated macrophages compared with the other two groups of macrophages (Figure 4A, $*P<0.05$). As shown in Figure 4B, HIF-1α protein expression was increased by 1.37±0.04-fold (n=3) under hypoxia and was reduced by 0.43±0.03-fold (n=3) in the presence of 27.2 μg/mL CNMs compared with the control. NF-κB p65 and phospho-NF-κB p65 protein expression was increased by 1.17±0.06-fold and 1.57±0.06-fold (n=3), respectively, under hypoxia and was decreased by 0.17±0.02-fold and 0.27±0.06-fold (n=3) after CNM treatment. Furthermore, p38 MAPK and phospho-p38

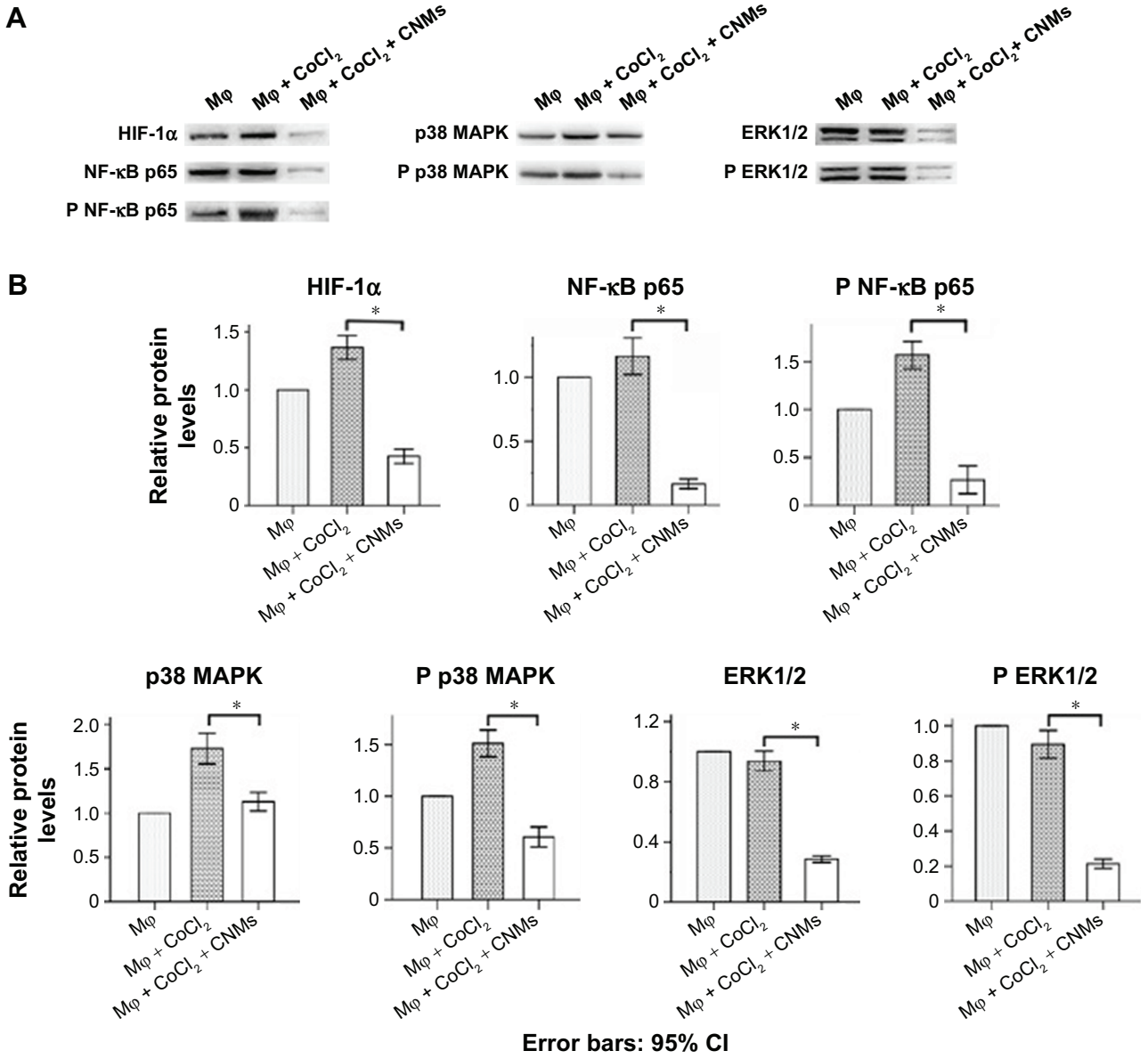

Figure 4 Effects of CNMs on the HIF-1α, NF-κB, and MAPKs pathways in hypoxia-inducing Mφ.

Notes: Mφ were incubated in the presence or absence of 27.2 μg/mL CNMs for 24 hours under normal or hypoxic ($CoCl_2$) conditions. HIF-1α, NF-κB p65, phospho-NF-κB p65, p38 MAPK, phospho-p38 MAPK, extracellular signal-regulated kinase-1/2 (ERK1/2), and phospho-ERK1/2 protein levels were detected by western blotting. (**A**) Shows one representative western blot of three independent experiments. (**B**) Show the relative protein levels and the statistical analysis results (mean values ± SD). Cytosolic and nuclear fractions under normal conditions without CNMs were set as 1, $*P<0.05$.

Abbreviations: CNMs, celastrol nanomicelles; ERK1/2, extracellular signal-regulated kinase 1/2; HIF-1α, hypoxia-inducible factors-1α; Mφ, macrophages; MAPKs, mitogen-activated protein kinase; NF-κB, nuclear factor-kappa B; NF-κB p65, nuclear factor-kappa B p65; phospho-NF-κB p65, phospho-nuclear factor-kappa B p65; p38 MAPK, p38 mitogen-activated protein kinase.

MAPK protein expression was increased by 1.73±0.07-fold and 1.51±0.05-fold (n=3), respectively, under hypoxia and was decreased by 1.13±0.04-fold and 0.61±0.04-fold (n=3) after CNM treatment (*$P<0.05$). ERK1/2 and phospho-ERK1/2 protein expression was nearly as high as that observed under hypoxia for 24 hours, whereas their expression was suppressed by 0.29±0.01-fold and 0.21±0.01-fold (n=3), respectively, following treatment with 27.2 μg/mL CNMs for 24 hours (*$P<0.05$).

The hypoxia-inducible factors have been identified as key mediators of angiogenesis and inflammation.[31] HIF-1α is an important inducer of VEGF in macrophages. Koide et al[32] showed that NF-κB activation is required for lipopolysaccharide (LPS)-induced HIF-1α expression and triggers VEGF production. The NF-κB pathway is also a key regulator of cytokine stimulation and angiogenesis, and this cytokine has been associated with inflammation, proliferation, invasion, metastasis, and angiogenesis.[21,33] The activation of NF-κB increased the secretion of several cytokines, such as TNF-α, VEGF, and MMP-9.[21,34] The MAPK pathway is closely associated with the regulation of inflammation.[35] As an important member of the MAPK family, p38 MAPK enhances NF-κB transactivation and also directly affect LPS-induced VEGF transcription in macrophages.[32] A recent study has shown that the p38 MAPK and ERK1/2 pathways are involved in the regulation of MMP-9 secretion in human osteosarcoma and human neuroblastoma cells.[36,37] A previous study showed that celastrol inhibited LPS-induced angiogenesis and blocked the nuclear translocation of the p65 subunit.[21] In the present study, the results indicated that treatment with CNMs remarkably decreased the $CoCl_2$-stimulated excessive release of VEGF, MCP-1, CINC3, and TNF-α by macrophages, which exerted its function by the downregulating MAPK, NF-κB activation, and HIF-1α expression. This effect might be the basis for the downregulation of cytokine, proinflammatory mediator, and chemokine secretion and the inhibition of angiogenesis.

Peritoneal cells elicited by mineral oil were highly purified macrophages

We used immunofluorescence to determine the immunochemical features of cells collected from the peritoneal cavity. The peritoneal cells were strongly immunoreactive for CD68 (Figure 5A). Figure 5A shows that the cytomembranes of the DiI-labeled macrophages exhibited red fluorescence. To analyze the purity and phagocytic activity of macrophages, we examined the internalization of FITC-labeled dextran through FACS. The percentage of endocytosing cells was 98.0%±0.4% (Figure 5B). The average percentage of DiI-labeled macrophages was on average 98.6%±0.5%, and that of macrophages treated with CNMs was on average 98.9%±0.3% (Figure 5C). Control macrophages were incubated with PBS.

In the present study, the cells elicited using mineral oil are considered as highly purified macrophages because of their uptake and expression of CD68 (ED1), which is a marker of macrophages in rats.[38] In a previous study, we demonstrated that the macrophages elicited using mineral oil exhibited an activated state and high expression of VEGF, platelet-derived growth factor, MMP-9, MMP-7, MMP-12, transforming growth factor β, and cyclooxygenase-2. These angiogenesis-associated mediators might help regulate new vessel formation, and subsequently, we observed that the activated macrophages significantly induced CNV when implanted into the rat corneal pocket. However, further study indicated that only MMP-9 and VEGF expression were distinctly increased in corneal tissue after macrophage implantation,[5] suggesting that the upregulation of MMP-9 and VEGF might be the major reason why activated macrophages induced CNV in the corneal pocket model.

CNMs suppress CNV induced by activated macrophages in the rat corneal pocket

We used the rat corneal micro-pocket assay to examine the antiangiogenic effect of CNMs in vivo. We observed corneal changes under the slit lamp after DiI-labeled macrophage implantation. New blood vessel buds appeared and began to invade into the corneal stroma on day 1 or 2 after surgery, and neovascularization peaked and began to regress after day 5 in the Mφ group (Figure 6). In the control group (treatment with PBS), only a few short capillaries appeared on day 1 and then began to disappear. Furthermore, there were only a few short CNVs on day 5 after surgery in the CNMs group. Corneal vessels were clearly visualized after ink perfusion on day 5 in each group (Figure 6A). We compared the mean length and area of CNV among the groups after ink perfusion corneal imaging. The mean length of CNV was 0.72±0.12 mm and 0.19±0.03 mm in the Mφ and control groups, respectively (Figure 6B, *$P<0.05$, **$P<0.01$). The mean area of CNV was 2.84±0.31 mm^2 and 0.79±0.12 mm^2 in the Mφ and control groups (Figure 6B), respectively, and the length and area of CNV were, respectively, significantly decreased in the CNMs group compared with the Mφ group (length of CNV: 0.33±0.04 mm, $P<0.01$ vs Mφ group and area of CNV: 1.40±0.29 mm^2, $P<0.01$ vs Mφ group).

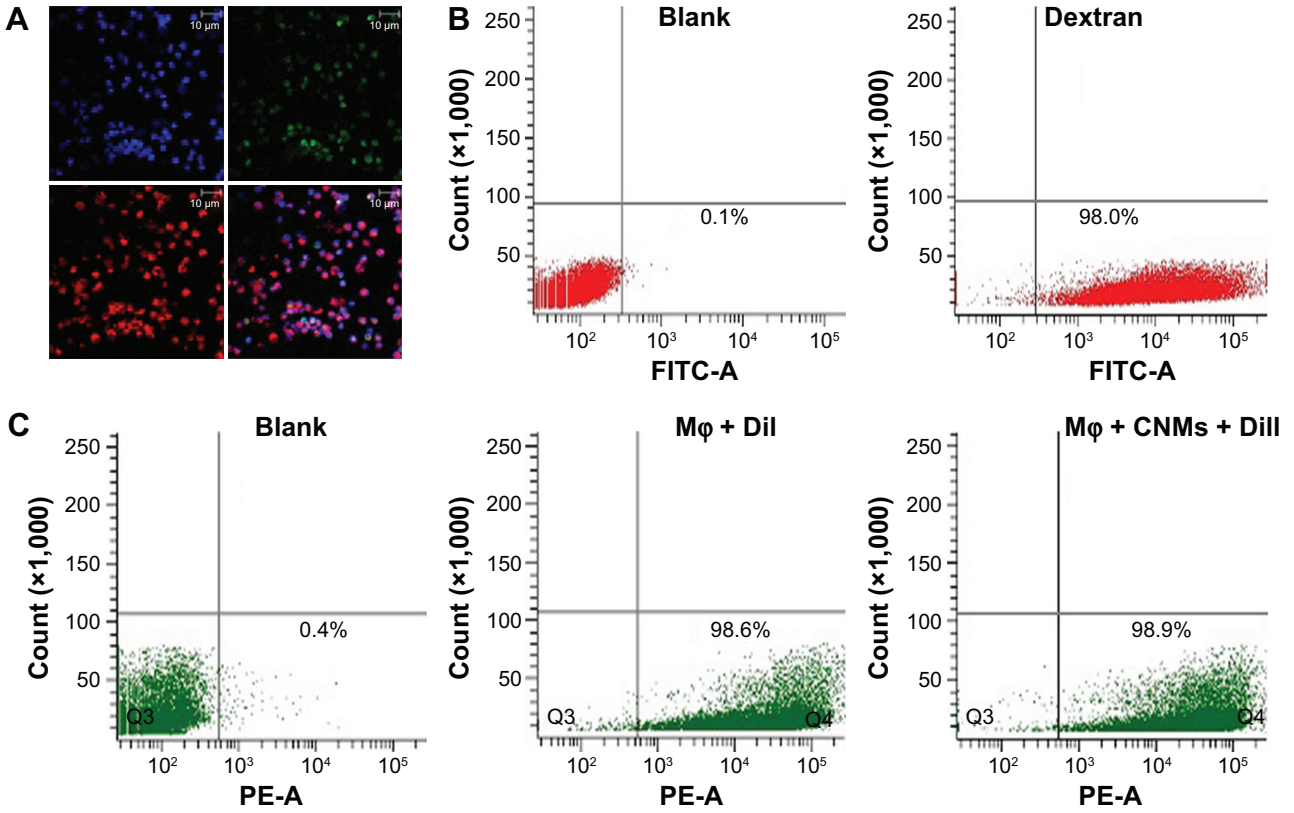

Figure 5 The identification, purity, and trace of Mφ.

Notes: The peritoneal cells elicited through mineral oil were highly purified Mφ. Immunofluorescence staining for the expression of specific antigens of Mφ was used to identify the cells collected from the peritoneal cavity. (**A**) Micrograph represents strong immunoreactivity for CD68. Antigens of CD68 are labeled green, nuclei are labeled blue, and DiI is labeled red. Each figure is at a magnification of ×400. The purity and phagocytic activity of Mφ were determined based on FITC-dextran positivity by fluorescence-activated cell sorting, and the percentage of endocytosing cells was 98.0%±0.4% (**B**). Flow cytometry analysis was used to analyze the proportions of cells harvested from peritoneal lavage fluids labeled with DiI. (**C**) The rate of DiI-labeled Mφ was 98.6%±0.5%, and that of Mφ treated with CNMs was 98.9%±0.3%. The Mφ were incubated with phosphate-buffered saline as a control.

Abbreviations: CD68, cluster of differentiation 68; CNMs, celastrol nanomicelles; DiI, 1,19-dioctadecyl-3-3-39,39-tetramethylindocarbocyanine; FITC-dextran, fluorescein isothiocyanate-dextran; Mφ, macrophages.

Macrophages play a vital role in CNV pathogenesis. In a previous study, we showed increased macrophage infiltration in CNV induced by suturing, whereas CNMs significantly decreased CNV and cell infiltration in rat corneas.[11] To investigate whether CNMs inhibited CNV through the inhibition of macrophages, we used the corneal pocket CNV model induced by macrophages. In this present study, we observed that the length and area of CNV were significantly reduced in the CNMs-treated group compared with the control group, indicating that CNMs can significantly inhibit CNV induced by activated macrophages.

In vivo fluorescence imaging and the effect of CNMs on VEGF and MMP-9 expression in rat cornea

DiI labeling was used to trace the macrophages implanted in the rat cornea. Figure 7A shows the fluorescence images in the cornea pocket on postoperative day 1. There were some DiI-labeled macrophages located in cornea pockets on postoperative day 1 in both the Mφ and CNMs groups, and there were no DiI-labeled cells in the corneal pocket in the control (PBS) group.

We further evaluated VEGF and MMP-9 protein expression in the corneas on postoperative day 2 in each group by immunofluorescence analysis. Obviously, high VEGF and MMP-9 expression was detected in the implanted DiI-labeled macrophages, corneal stroma, and corneal endothelium of the Mφ group (Figure 7B). In contrast, the control group showed no remarkable expression of MMP-9 and VEGF in the cornea, and there was a significant reduction in MMP-9 and VEGF expression in implanted DiI-labeled macrophage, as well as the corneal stroma and corneal endothelium (Figure 7B).

Macrophages are infiltrating inflammatory cells in many types of tumor that promotes tumor progression via the enhancement of tumor angiogenesis. Macrophages

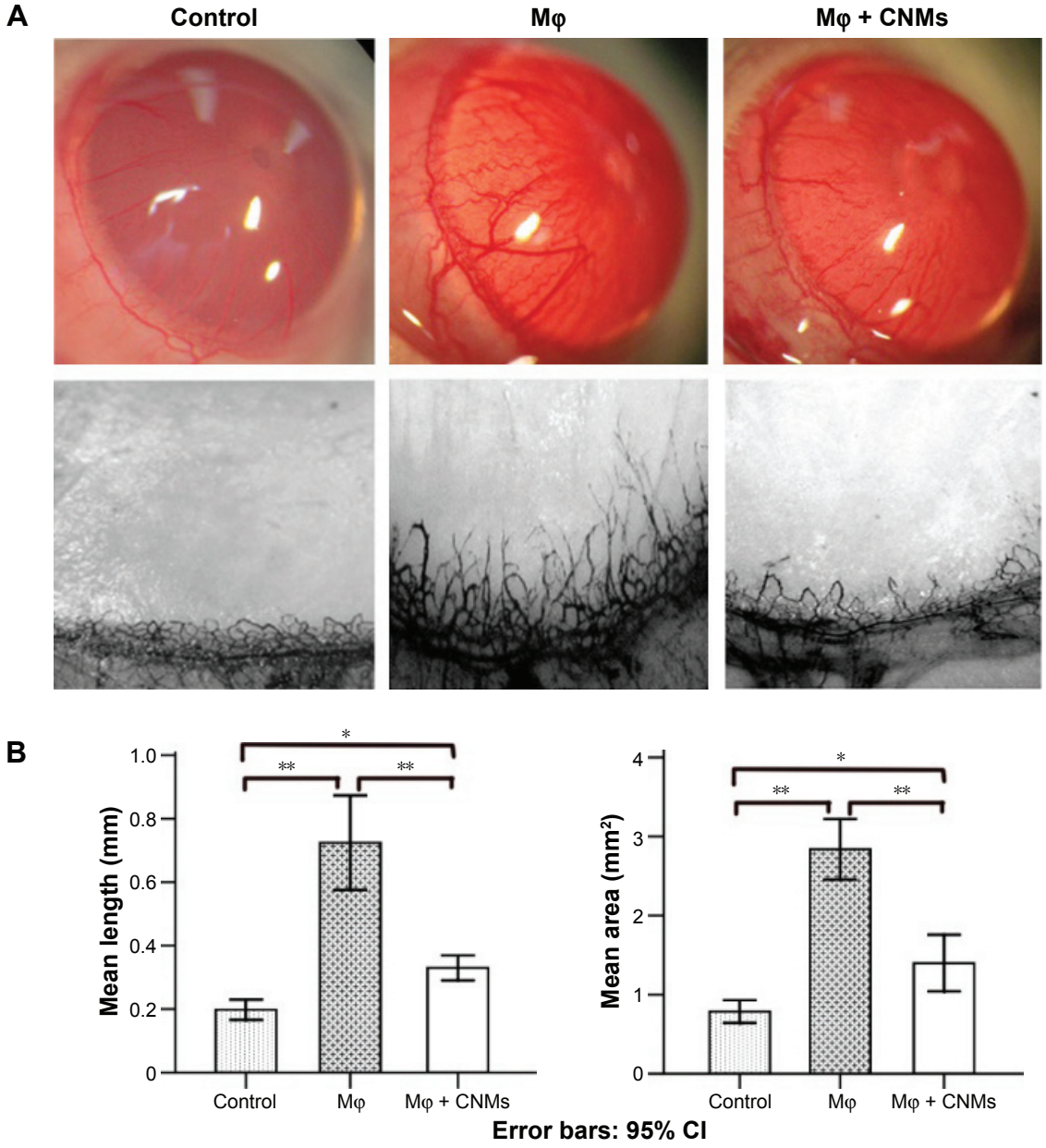

Figure 6 CNMs suppress CNV induced by Mφ in a rat corneal pocket model.
Notes: Cells labeled with 1,19-dioctadecyl-3-3-39,39-tetramethylindocarbocyanine were implanted into a surgically created corneal micro-pocket in the right eye of SD rats. On day 5, the CNVs were visualized by ink angiography. (**A**) Abundant CNVs grew from the limbus toward the pocket in the Mφ group, whereas there was obviously less angiogenesis in the CNMs group. However, angiogenesis was noticeably less in the phosphate-buffered saline group. Magnification ×25. (**B**) The mean length and area of CNV in the CNMs group were much less than that in the Mφ group. *$P<0.05$, **$P<0.01$.
Abbreviations: CI, confidence interval; CNMs, celastrol nanomicelles; CNV, corneal neovascularization; Mφ, macrophage; SD, Sprague-Dawley.

enhanced proangiogenic activity of breast cancer cells via the induction of VEGF and MMP-9.[39] In CNV, previous data indicated that activated macrophages induced CNV through the upregulation of VEGF and MMP-9.[5] Celastrol inhibited angiogenesis-mediated tumor growth and alleviated macrophage-mediated inflammation.[20,40] The results of the present study demonstrated that CNMs suppressed the expression of VEGF and MMP-9 in activated macrophages and corneal tissue, suggesting that CNMs might inhibit CNV by downregulation of the secretion activity of macrophages, which is consistent with the in vitro experimental result.

Conclusion

In the present study, we demonstrated the targeting of CNMs to hypoxia-induced macrophages. Inhibition of p38

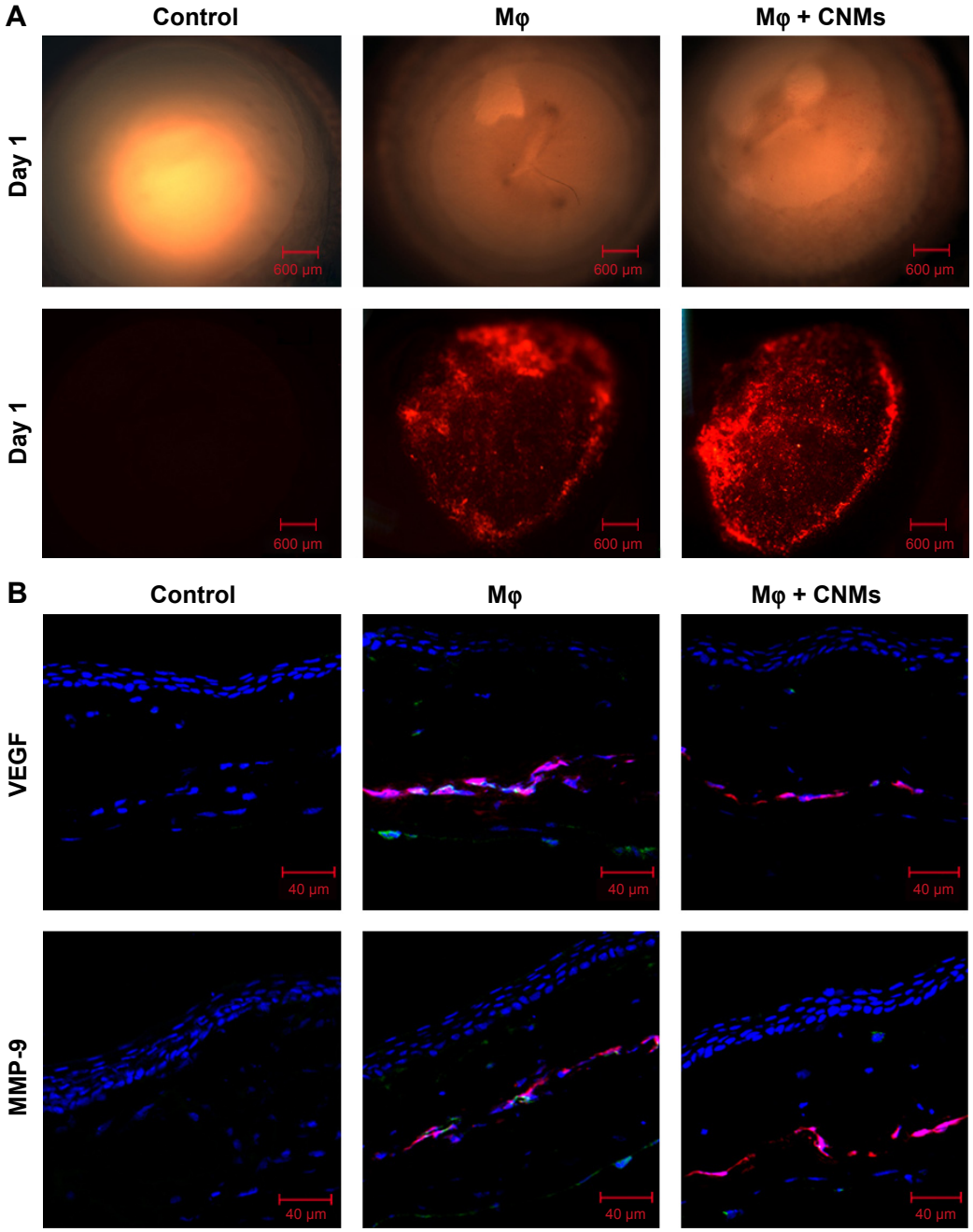

Figure 7 In vivo fluorescence imaging and effect of CNMs on VEGF and MMP-9 expression in rat cornea.
Notes: (**A**) Fluorescence micrographs of a cornea indicate the Mφ labeled with DiI located in cornea pockets on postoperative day 1 in the Mφ group and CNMs group. There were no DiI-labeled cells in the cornea pocket in the control group. Magnification ×25. (**B**) Confocal laser scanning microscopic images of a cornea indicate the protein expression of VEGF and MMP-9 on postoperative day 2. Visibly high expression of VEGF and MMP-9 was observed in implanted DiI-labeled Mφ, corneal stroma, and corneal endothelium in the Mφ group. There was a significant reduction in VEGF and MMP-9 expression in implanted Mφ and corneal stroma and endothelium in the CNMs group. No remarkable expression of VEGF and MMP-9 was observed in the control group.
Abbreviations: CNMs, celastrol nanomicelles; DiI, 1,19-dioctadecyl-3-3-39,39-tetramethylindocarbocyanine; Mφ, macrophage; MMP-9, matrix metalloproteinases 9; VEGF, vascular endothelial growth factor.

MAPK, ERK1/2, and NF-κB activation and the expression of HIF-1α pathway components by CNM treatment resulted in the suppression of MCP-1, TNF-α, VEGF, and MMP-9 expression in macrophages. These findings indicate that CNMs inhibit CNV induced by activated macrophages in the rat corneal pocket model, proposing a new therapeutic target for celastrol. The limitation of the present study is that we did not try to investigate the different polarization states of macrophages treated with or without celastrol in the presence of CNV. Thus, future studies are needed to evaluate the cell toxicity and eye irritation associated with CNMs.

Acknowledgment

This work was supported by grants from the Natural Science Foundation of China (U1304811, 81600775, 21504082, 81270991, and 81271051).

Disclosure

The authors report no conflicts of interest in this work.

References

1. Safvati A, Cole N, Hume E, Willcox M. Mediators of neovascularization and the hypoxic cornea. *Curr Eye Res*. 2009;34(6):501–514.
2. Chang JH, Gabison EE, Kato T, Azar DT. Corneal neovascularization. *Curr Opin Ophthalmol*. 2001;12(4):242–249.
3. Ferrara N, Gerber HP, LeCouter J. The biology of VEGF and its receptors. *Nat Med*. 2003;9(6):669–676.
4. Risau W. Mechanisms of angiogenesis. *Nature*. 1997;386(6626):671–674.
5. Li ZR, Li YP, Lin ML, et al. Activated macrophages induce neovascularization through upregulation of MMP-9 and VEGF in rat corneas. *Cornea*. 2012;31(9):1028–1035.
6. Yang L, Li Y, Ren J, et al. Celastrol attenuates inflammatory and neuropathic pain mediated by cannabinoid receptor type 2. *Int J Mol Sci*. 2014;15(8):13637–13648.
7. Ma J, Han LZ, Liang H, et al. Celastrol inhibits the HIF-1α pathway by inhibition of mTOR/p70S6K/eIF4E and ERK1/2 phosphorylation in human hepatoma cells. *Oncol Rep*. 2014;32(1):235–242.
8. Kannaiyan R, Shanmugam MK, Sethi G. Molecular targets of celastrol derived from Thunder of God Vine: potential role in the treatment of inflammatory disorders and cancer. *Cancer Lett*. 2011;303(1):9–20.
9. Salminen A, Lehtonen M, Paimela T, Kaarniranta K. Celastrol: molecular targets of thunder god vine. *Biochem Biophys Res Commun*. 2010;394(3):439–442.
10. Liu J, Lee J, Salazar HMA, Mazitschek R, Ozcan U. Treatment of obesity with celastrol. *Cell*. 2015;161(5):999–1011.
11. Li Z, Yao L, Li J, et al. Celastrol nanoparticles inhibit corneal neovascularization induced by suturing in rats. *Int J Nanomedicine*. 2012;7:1163–1173.
12. Lin ML, Li YP, Li ZR, Lin JX, Zhou XL, Liang D. Macrophages acquire fibroblast characteristics in a rat model of proliferative vitreoretinopathy. *Ophthalmic Res*. 2011;45(4):180–190.
13. Pang X, Yi T, Yi Z, et al. Morelloflavone, a biflavonoid, inhibits tumor angiogenesis by targeting rho GTPases and extracellular signal-regulated kinase signaling pathways. *Cancer Res*. 2009;69(2):518–525.
14. Mao Y, Wang B, Xu X, Du W, Li W, Wang Y. Glycyrrhizic acid promotes M1 macrophage polarization in murine bone marrow-derived macrophages associated with the activation of JNK and NF-κB. *Mediators Inflamm*. 2015;2015:372931.
15. Yao L, Li ZR, Su WR, et al. Role of mesenchymal stem cells on cornea wound healing induced by acute alkali burn. *PLoS One*. 2012;7(2):e30842.
16. Li Z, Wu X, Li J, et al. Antitumor activity of celastrol nanoparticles in a xenograft retinoblastoma tumor model. *Int J Nanomedicine*. 2012;7:2389–2398.
17. Sanna V, Chamcheu JC, Pala N, Mukhtar H, Sechi M, Siddiqui IA. Nanoencapsulation of natural triterpenoid celastrol for prostate cancer treatment. *Int J Nanomedicine*. 2015;10:6835–6846.
18. Li W, Zhang T, Ye Y, Zhang X, Wu B. Enhanced bioavailability of tripterine through lipid nanoparticles using broccoli-derived lipids as a carrier material. *Int J Pharm*. 2015;495(2):948–955.
19. Li J, Li Z, Zhou T, et al. Positively charged micelles based on a triblock copolymer demonstrate enhanced corneal penetration. *Int J Nanomedicine*. 2015;10:6027–6037.
20. Pang X, Yi Z, Zhang J, et al. Celastrol suppresses angiogenesis-mediated tumor growth through inhibition of AKT/mammalian target of rapamycin pathway. *Cancer Res*. 2010;70(5):1951–1959.
21. Ni H, Zhao W, Kong X, Li H, Ouyang J. Celastrol inhibits lipopolysaccharide-induced angiogenesis by suppressing TLR4-triggered nuclear factor-kappa B activation. *Acta Haematol*. 2014;131(2):102–111.
22. Voiculescu OB, Voinea LM, Alexandrescu C. Corneal neovascularization and biological therapy. *J Med Life*. 2015;8(4):444–448.
23. Shweta, Mishra KP, Chanda S, Singh SB, Ganju L. A comparative immunological analysis of $CoCl_2$ treated cells with in vitro hypoxic exposure. *Biometals*. 2015;28(1):175–185.
24. Szade A, Grochot-Przeczek A, Florczyk U, Jozkowicz A, Dulak J. Cellular and molecular mechanisms of inflammation-induced angiogenesis. *IUBMB Life*. 2015;67(3):145–159.
25. Su W, Li Z, Li Y, et al. Doxycycline enhances the inhibitory effects of bevacizumab on corneal neovascularization and prevents its side effects. *Invest Ophthalmol Vis Sci*. 2011;52(12):9108–9115.
26. Lin Y, Ma Q, Lin S, et al. Inhibitory effects of (90)Sr/(90)Y β-irradiation on alkali burn-induced corneal neovascularization in rats. *Exp Ther Med*. 2016;11(2):409–414.
27. Wang Y, Yin H, Chen P, Xie L, Wang Y. Inhibitory effect of canstatin in alkali burn-induced corneal neovascularization. *Ophthalmic Res*. 2011;46(2):66–72.
28. Chang JH, Garg NK, Lunde E, Han KY, Jain S, Azar DT. Corneal neovascularization: an anti-VEGF therapy review. *Surv Ophthalmol*. 2012;57(5):415–429.
29. Salacz ME, Kast RE, Saki N, Brüning A, Karpel-Massler G, Halatsch ME. Toward a noncytotoxic glioblastoma therapy: blocking MCP-1 with the MTZ Regimen. *Onco Targets Ther*. 2016;9:2535–2545.
30. Gu P, Qiu FC, Han R, et al. Efficient differentiation of neural stem cells induced by the rat bone marrow stromal cells. *Int J Clin Exp Med*. 2015;8(5):6713–6724.
31. Nath B, Szabo G. Hypoxia and hypoxia inducible factors: diverse roles in liver diseases. *Hepatology*. 2012;55(2):622–633.
32. Koide N, Odkhuu E, Naiki Y, et al. Augmentation of LPS-induced vascular endothelial cell growth factor production in macrophages by transforming growth factor-β1. *Innate Immun*. 2014;20(8):816–825.
33. Pollet I, Opina CJ, Zimmerman C, Leong KG, Wong F, Karsan A. Bacterial lipopolysaccharide directly induces angiogenesis through TRAF6-mediated activation of NF-kappaB and c-Jun N-terminal kinase. *Blood*. 2003;102(5):1740–1742.
34. Wang G, Tian W, Liu Y, et al. Visfatin triggers the cell motility of non-small cell lung cancer (NSCLC) via up-regulation of matrix metalloproteinases (MMPs). *Basic Clin Pharmacol Toxicol*. Epub 2016 May 25.
35. Xue J, Chen F, Wang J, et al. Emodin protects against concanavalin A-induced hepatitis in mice through inhibiting activation of the p38 MAPK-NF-κB signaling pathway. *Cell Physiol Biochem*. 2015;35(4):1557–1570.
36. Su Y, Wan D, Song W. Dryofragin inhibits the migration and invasion of human osteosarcoma U2OS cells by suppressing MMP-2/9 and elevating TIMP-1/2 through PI3K/AKT and p38 MAPK signaling pathways. *Anticancer Drugs*. 2016;27(7);660–668.
37. Yang CC, Hsiao LD, Yang CM, Lin CC. Thrombin enhanced matrix metalloproteinase-9 expression and migration of SK-N-SH Cells via PAR-1, c-Src, PYK2, EGFR, ERK1/2 and AP-1. *Mol Neurobiol*. Epub 2016 May 16.
38. Seifart C, Muyal JP, Plagens A, et al. All-trans retinoic acid results in irregular repair of septa and fails to inhibit proinflammatory macrophages. *Eur Respir J*. 2011;38(2):425–439.
39. Lee CC, Liu KJ, Wu YC, Lin SJ, Chang CC, Huang TS. Sesamin inhibits macrophage-induced vascular endothelial growth factor and matrix metalloproteinase-9 expression and proangiogenic activity in breast cancer cells. *Inflammation*. 2011;34(3):209–221.
40. Cascão R, Vidal B, Lopes IP, et al. Decrease of CD68 synovial macrophages in celastrol treated arthritic rats. *PLoS One*. 2015;10(12):e0142448.